Journal of Luminescence 157 (2015) 197–200

Contents lists available at ScienceDirect

Journal of Luminescence

journal homepage: www.elsevier.com/locate/jlumin

Preparation and luminescence properties of $Sr_2Eu_xLa_{1-x}AlO_5$ phosphor

Xiaoyuan Sun [a,*], Chunjie Li [a], Xiaoguang He [a], Lijun Yu [a], Haiyan Qi [a], Yunfeng Gao [a], Feng Gao [a], Chunlei Wu [b], Yongshi Luo [c], Jiahua Zhang [c]

[a] Department of Physics, Changchun Normal University, Changchun 130032, China
[b] Faculty of Science, Mudanjiang Normal University, Mudanjiang 157012, China
[c] Key Laboratory of Luminescence and Application, Changchun Institute of Optics, Fine Mechanics and Physics, Chinese Academy of Science, Changchun 130033, China

ARTICLE INFO

Article history:
Received 29 July 2013
Received in revised form
24 August 2014
Accepted 27 August 2014
Available online 9 September 2014

Keywords:
Photoluminescence
Phosphor
White light emitting diode

ABSTRACT

The red emitting phosphor Sr_2EuAlO_5 was synthesized through the solid state reaction technique. The strong red emission of Eu^{3+} peaks around 590 nm and 620 nm was observed. The photoluminescence excitation spectra show a broad O^{2-}–Eu^{3+} charge-transfer band in UV region and f–f transitions in near UV and visible region. By adding La^{3+} into the Sr_2EuAlO_5 phosphor, the red emission enhancement was observed. The luminescence lifetime and external quantum efficiency of these phosphors were measured. The Chromaticity Coordinates of $Sr_2Eu_{0.75}La_{0.25}AlO_5$ is $x=0.64$, $y=0.36$. The characteristic index shows that the red emission phosphor has high color saturation.

© 2014 Elsevier B.V. All rights reserved.

1. Introduction

Growing interest has been focused on white light emitting diodes (LEDs) in recent years. White LEDs are considered the next-generation light source as a consequence of their energy-saving, long lifetimes, maintenance and safety [1–5]. The most common method to realize white LED is to combine a blue chip with a yellow phosphor material, such as YAG:Ce^{3+}. However, this kind of white LED is not suitable for applications requiring high color rendering properties, such as residential and medical lighting [6,7]. Another approach might solve this problem by using a near UV LED chip coated with corresponding phosphors to generate warm white light. This approach provides white LEDs with excellent color rendering indexes and higher color stability [8–10]. Because near UV light is less sensitive to the human eye than blue light, all the colors are determined by the phosphors. Therefore, phosphor materials play an important role in white LEDs. Up to now, red phosphors suitable for near UV excitation with better optical properties are still in development.

Eu^{3+}-doped materials, especially in which the Eu^{3+} ions occupy a non-centrosymmetric site in the host, have been widely used as the red emitting phosphors due to their intense $^5D_0$–$^7F_2$ emission in the red spectral region [11–14]. In the present work, a red emitting phosphor, Sr_2EuAlO_5, has been synthesized. The strong red emission around 620 nm was obtained. Eu^{3+} ion is as host, also as activator in Sr_2EuAlO_5 phosphor. Thus, the concentration quenching may occur for high Eu^{3+} concentration. La^{3+} ion with no 4f electrons, has no electronic energy levels that can induce excitation and luminescence processes in or near the visible region. Further, the ionic radii of La^{3+} (1.160 Å) and Eu^{3+} (1.066 Å) are similar. Thus, we substituted La^{3+} ion for Eu^{3+} ion, and expected that the progressive replacement of Eu^{3+} by La^{3+} in the photoluminescence property. With this in view, a series of red emitting phosphors $Sr_2Eu_xLa_{1-x}AlO_5$ ($x=0.05$–1.0) were synthesized by high temperature solid state reaction and its crystalline structure, photoluminescence properties, fluorescence lifetime and external quantum efficiency were investigated.

2. Experimental

Polycrystalline powder samples of $Sr_2Eu_xLa_{1-x}AlO_5$ ($x=0.05$, 0.1, 0.15, 0.25, 0.35, 0.5, 0.75, and 1.0) and $Sr_3Al_2O_6$:Eu^{3+} phosphors have been synthesized through the high temperature solid state reaction technique. The $SrCO_3$ (99%), La_2O_3 (99.99%), Eu_2O_3 (99.99%), and Al_2O_3 (99.99%) were employed as the raw materials. These raw materials in the desired ratio were well milled, then transferred to an alumina crucible. The mixture was fired at 1400 °C for 4 h in an electric furnace, and cooled slowly to room temperature. The final phase was checked using a Japan Rigaku D/max-rA powder X-ray diffractometer with monochromatized Cu KR radiation ($\lambda=0.15406$ Å). The photoluminescence (PL) and the photoluminescence excitation (PLE) spectra were measured with

* Corresponding author. Tel./fax: +86 431 8616 8078.
E-mail address: sxueyuan@163.com (X. Sun).

http://dx.doi.org/10.1016/j.jlumin.2014.08.052
0022-2313/© 2014 Elsevier B.V. All rights reserved.

a Hitachi F-4600 Spectral spectrophotometer equipped with a xenon lamp. The external quantum efficiency was analyzed with a Hitachi F-7000 Spectral spectrophotometer under excitation at 300 nm and 393 nm. In fluorescence lifetime measurements, the third harmonic (355 nm) of a Nd doped yttrium aluminum garnet laser (Spectra-Physics, GCR 130) was used as an excitation source, and the signals were detected with a Tektronix digital oscilloscope (TDS 3052).

3. Results and discussion

3.1. X-ray diffraction analysis

The X-ray diffraction patterns of $Sr_2Eu_xLa_{1-x}AlO_5$ (x=0.05, 0.1, 0.25, 0.35, 0.5, 0.75, and 1.0) phosphors are shown in Fig. 1. The X-ray diffraction pattern of Sr_2EuAlO_5 agrees well with JCPDS 70-2197, indicating that the obtained sample is in a single phase. Sr_2EuAlO_5 are tetragonal, space group I4/mcm and Z=4. Cell parameters are a=6.742(1) Å and c=10.970(1) Å [15]. Because the ionic radii of 8-coordinate La^{3+} (1.160 Å) and Eu^{3+} (1.066 Å) differ only moderately [16], the crystal structure of $Sr_2Eu_xLa_{1-x}AlO_5$ (x=0.05, 0.1, 0.25, 0.35, 0.5, and 0.75) phosphors is in common with Sr_2EuAlO_5. In Fig. 1, it can be seen that there is a little shift in the peak toward left with increase in La^{3+} concentration, indicating the lattice distortion. The variation should arise from the ionic radii difference of Eu^{3+} (r=1.066 Å when coordination number (CN)=8) and La^{3+} (r=1.160 Å when CN=8). By the Bragg formula

$$2d \sin\theta = n\lambda \quad (1)$$

where d is the distance of crystal lattice, θ is the diffraction angle, n is a positive integer, and λ is the X-ray wavelength. According to the Bragg formula, the distance of crystal lattice increases with increasing the La^{3+} concentration. The crystal lattice of $Sr_2Eu_xLa_{1-x}AlO_5$ would expand due to the longer bond length of La–O compared to that of Eu–O. Some impure phase peaks appear when the x value is less than 0.35. The Sr_2EuAlO_5 crystal structure maintains unchanged with the Eu^{3+} concentration up to x=0.5. According to JCPDS card (no. 03-0741), the impure phase peaks arise from $Sr_3Al_2O_6$ phosphor

3.2. PLE and PL spectra of $Sr_2Eu_xLa_{1-x}AlO_5$

The PLE spectra of $Sr_2Eu_xLa_{1-x}AlO_5$ (x=0.05, 0.25, 0.5, and 1.0) phosphors, monitoring the $^5D_0$–$^7F_2$ are presented in Fig. 2. The PLE

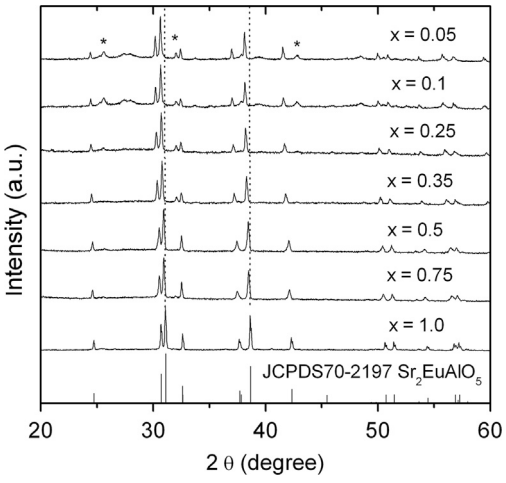

Fig. 1. X-ray diffraction patterns of the $Sr_2Eu_xLa_{1-x}AlO_5$ (x=0.05, 0.1, 0.25, 0.35, 0.5, 0.75, and 1.0) phosphors.

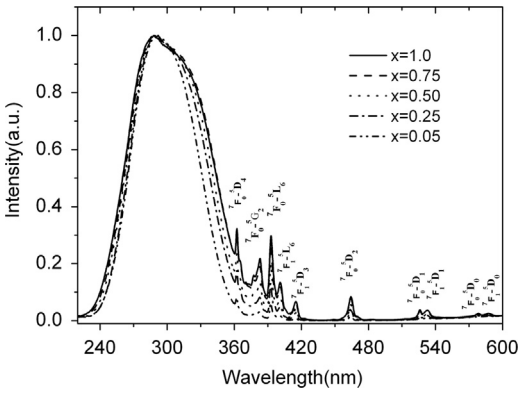

Fig. 2. PLE spectra of the $Sr_2Eu_xLa_{1-x}AlO_5$ (x=0.05, 0.25, 0.5, and 1.0) phosphors.

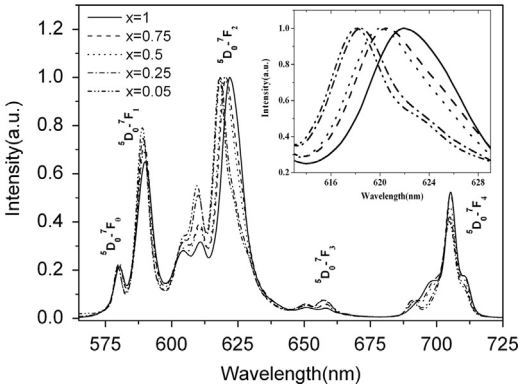

Fig. 3. PL spectra of $Sr_2Eu_xLa_{1-x}AlO_5$ phosphor. Inset shows the zoom of the $^5D_0$–$^7F_2$ transitions.

spectra of the Eu^{3+} ion consist of a strong broad band, which is due to a charge-transfer (CT) band of the ligand to metal CT state from the O^2–Eu^{3+}. Additional sharp peaks are observed between 360 and 540 nm, which are due to f–f electronic transitions of Eu^{3+} ions [17]. The intensity of the CT band is higher than that of the f–f transitions. The CT bands of the phosphors for the $^5D_0 \rightarrow {}^7F_2$ emission of Eu^{3+} ions center at about 300 nm. The spectra show narrow excitation lines at longer wavelengths corresponding to the characteristic f–f transitions of Eu^{3+}; these lines are assigned as follows: $^7F_0 \rightarrow {}^5D_4$ (362 nm), $^7F_0 \rightarrow {}^5G_2$ (383 nm), $^7F_0 \rightarrow {}^5L_6$ (393 nm), $^7F_1 \rightarrow {}^5L_6$ (401 nm), $^7F_1 \rightarrow {}^5D_3$ (415 nm), $^7F_0 \rightarrow {}^5D_2$ (464 nm), $^7F_0 \rightarrow {}^5D_1$ (526 nm), $^7F_1 \rightarrow {}^5D_1$ (533 nm), $^7F_0 \rightarrow {}^5D_0$ (578 nm) and $^7F_1 \rightarrow {}^5D_1$ (587 nm) [18]. The CT bands shift to longer wavelength with increasing Eu^{3+} concentrations from 0 to 1. The CT state transition energy is dependent on the covalence of ligand and rare ion [19]. The distance between ligand and rare ion is decrease with increasing the Eu^{3+} concentration. The nephelauxetic effect of electronic cloud increase and the covalence becomes strong. The field of O^{2-} site becomes weaker as the covalence become stronger. The CT bands shift to longer wavelength as the Eu^{3+} concentration increase.

The PL spectra of $Sr_2Eu_xLa_{1-x}AlO_5$ (x=1.0, 0.75, 0.5, 0.25, 0.05) under 310 nm excitation wavelength are presented in Fig. 3. These peaks could be assigned to the well-known transitions from the initial state $^5D_0$ to the final states ^7F_J (J=0–4) (signed in Fig. 3). Upon excitation with 310 nm UV irradiation, the photoluminescence spectra show three strong emission peaks around 590 nm, 620 nm and 705 nm, which arise from the $^5D_0 \rightarrow {}^7F_1$, $^5D_0 \rightarrow {}^7F_2$ and the $^5D_0 \rightarrow {}^7F_4$ transitions of Eu^{3+}, respectively. These emission lines are observed under either CT band or 393/464 nm excitation also. The emission around 620 nm is due to the $^5D_0 \rightarrow {}^7F_2$ electric dipole transition, which is induced by the lack of inversion symmetry at the Eu^{3+} site. The emission at 590 nm is due to the $^5D_0 \rightarrow {}^7F_1$ magnetic dipole

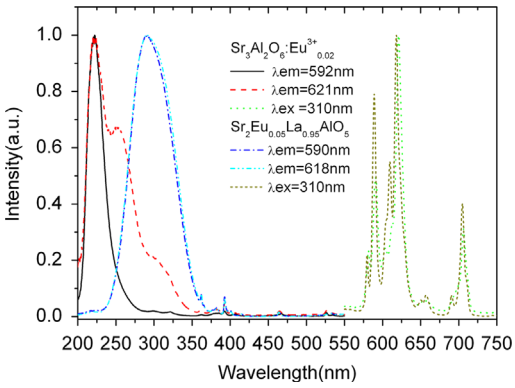

Fig. 4. PLE and PL spectra of $Sr_3Al_2O_6:Eu^{3+}_{0.02}$ and $Sr_2Eu_{0.05}La_{0.95}AlO_5$.

transitions, which is insensitive to the site symmetry. The emission intensity ratio of $^5D_0 \rightarrow {}^7F_2$ to $^5D_0 \rightarrow {}^7F_1$ transitions strongly depends on the local symmetry of the Eu^{3+} ions in host lattice. When the Eu^{3+} ions occupy symmetric sites, the ratio is smaller. The electric dipole transition $^5D_0 \rightarrow {}^7F_2$ is predominant, this indicates that Eu^{3+} ions occupy the non-inversion symmetric sites in the host lattice [17]. A zoom of the $^5D_0 \rightarrow {}^7F_2$ transitions is inserted in Fig. 3. It clearly exhibits that the emission peak shifts to the longer wavelength as Eu^{3+} concentration increases. When the distance between rare ion and ligand becomes shorter, nephelauxetic effect increase, the emission spectra show a red-shift [20]. The bond length of Eu–O is shorter than that of La–O, therefore, the emission bands shift to the longer wavelength side as Eu^{3+} concentration increases.

3.3. Comparison of luminescence intensities of $Sr_2Eu_{0.05}La_{0.95}AlO_5$ with $Sr_3Al_2O_6:Eu^{3+}$ phosphor

The PLE and PL spectra of $Sr_3Al_2O_6:Eu^{3+}_{0.02}$ and $Sr_2Eu_{0.05}La_{0.95}AlO_5$ are presented in Fig. 4. The $Sr_3Al_2O_6:Eu^{3+}$ phosphor exhibits narrow emission at 582 nm, 592 nm, 604 nm, 621 nm, and 706 nm. The strongest emission peaks at 621 nm. The CT band of $Sr_3Al_2O_6:Eu^{3+}$ for the $^5D_0 \rightarrow {}^7F_1$ emission of Eu^{3+} ions center at about 220 nm. When the $^5D_0$–$^7F_2$ transition of Eu^{3+} is monitored, three broad bands are observed. The strongest excitation peaks at around 220 nm. The PLE and PL spectra of $Sr_3Al_2O_6:Eu^{3+}$ are different from that of $Sr_2Eu_{0.05}La_{0.95}AlO_5$. Therefore, the PL in Fig. 3 should originate from $Sr_2Eu_xLa_{1-x}AlO_5$ phosphor mainly.

3.4. Dependence of PL intensities on Eu^{3+} concentrations in $Sr_2Eu_xLa_{1-x}AlO_5$

Fig. 5(a) and (b) depicts the dependence of the integrated luminescence intensities on Eu^{3+} concentration in $Sr_2Eu_xLa_{1-x}AlO_5$ (x=0.05, 0.15, 0.25, 0.35, 0.5, 0.75, and 1.0) under 300 nm and 393 nm excitation, respectively. The integrated luminescence intensities increase first and then decrease with an increase in Eu^{3+} concentration. The emission intensities reach a maximum around x=0.5 and x=0.75 when excited at 300 nm and 393 nm, respectively. The results imply that concentration quenching occurs for the emissions from high energy levels of Eu^{3+} ions in the case of high Eu^{3+} concentration. Therefore, the most efficient concentrations for the maximum red emission can be improved by substituting La^{3+} ions for Eu^{3+}. Moreover, substitution of La_2O_3 for Eu_2O_3 can reduce the raw material costs.

3.5. Quantum efficiency of $Sr_2Eu_xLa_{1-x}AlO_5$ phosphors

The external quantum efficiency of $Sr_2Eu_xLa_{1-x}AlO_5$ (x=0.25, 0.5, 0.75, and 1.0) phosphors is listed in Table 1 under excitation at 300 nm and 393 nm. The quantum efficiency increase first and

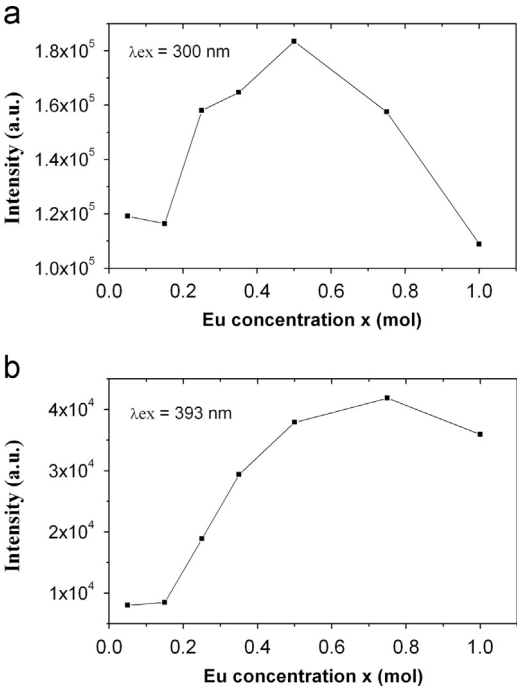

Fig. 5. Dependence of integrated emission intensity of $Sr_2Eu_xLa_{1-x}AlO_5$ on Eu^{3+} concentration under 300 nm (a) and 393 nm (b) excitation.

Table 1
Quantum efficiency of $Sr_2Eu_xLa_{1-x}AlO_5$ phosphors and $Y_2O_2S:Eu^{3+}$ red phosphor.

x	0.25	0.5	0.75	1.0	$Y_2O_2S:Eu^{3+}$
η (%) (λ_{ex}=300 nm)	42.7	43.3	36.2	16.3	59.1
η (%) (λ_{ex}=393 nm)	10.9	14.5	15.6	8.5	8.7

then decrease with an increase in Eu^{3+} concentration. The highest quantum efficiency values are found at x=0.5 and x=0.75 when excited at 300 nm and 393 nm, respectively. The maximum quantum efficiency is 43.3% when excited at 300 nm, and 15.6% when excited at 393 nm. The quantum efficiency is improved can be improved by substituting La^{3+} ions for Eu^{3+}.

3.6. Fluorescence lifetimes

The fluorescence decay curves of the Eu^{3+} ions in $Sr_2Eu_xLa_{1-x}AlO_5$ (x=0.05, 0.25, 0.5, 0.75, and 1.0) phosphors are measured with an excitation at 355 nm and monitored at 620 nm, as represented in Fig. 6. For the decay curves of the Eu^{3+} ions, the fluorescence decays deviate slightly from a single-exponential rule, indicating the presence of a non-radiative process. The lifetime can be calculated by the effective lifetime from Eq. (2):

$$\tau = \frac{\int_0^\infty I(t)tdt}{\int_0^\infty I(t)dt} \quad (2)$$

where $I(t)$ represents the luminescence intensity at a time t, and τ is the decay lifetime. Using this equation, the lifetime of the excited states in $Sr_2Eu_xLa_{1-x}AlO_5$ for different Eu^{3+} contents is calculated. The values of lifetime are calculated to be 315, 452, 594, 767, and 521 μs for x values of 0.05, 0.25, 0.5, 0.75, and 1.0, respectively. The lifetime values increase with an increase in the Eu^{3+} ion in the host matrix, then decrease, as shown in Fig. 6. The lifetimes are quenched at concentrations around x=0.75. The decrease in the lifetime can be attributed to energy transfer among Eu^{3+} ions nonradiately at higher concentration of Eu^{3+} ions in the Sr_2EuAlO_5 host matrix [21].

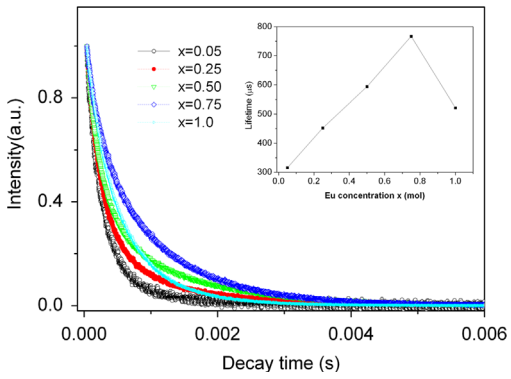

Fig. 6. PL decay curves of the Eu^{3+} ions in $Sr_2Eu_xLa_{1-x}AlO_5$ ($x=0.05$, 0.25, 0.5, 0.75, and 1.0) phosphors (excited at 355 nm, monitored at 620 nm). Inset shows lifetime with Eu^{3+} content.

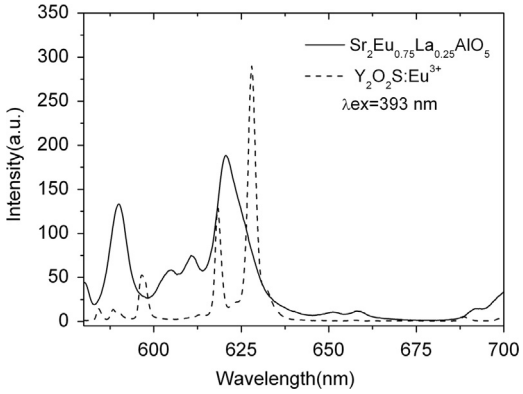

Fig. 7. PL spectra of $Sr_2Eu_{0.75}La_{0.25}AlO_5$ (solid line) and commercial $Y_2O_2S:Eu^{3+}$ red phosphors (dashed line) under 393 nm excitation.

3.7. Comparison of luminescence intensities of $Sr_2Eu_xLa_{1-x}AlO_5$ with commercial red phosphors

Y_2O_2S-doped with Eu^{3+} is a well-known red photoluminescent and cathodo-luminescent phosphor. At present, this phosphor is a red candidate for solid-state lighting application. The spectra upon 393 nm excitation in to the $^5L_6$ state monitoring at the red emission in $Sr_2Eu_{0.75}La_{0.25}AlO_5$ are compared with that of commercial $Y_2O_2S:Eu^{3+}$ red phosphors, as shown in Fig. 7. The integral emission intensity of the $^5D_0$–$^7F_2$ emission line of $Sr_2Eu_{0.75}La_{0.25}AlO_5$ is compared with the $Y_2O_2S:Eu^{3+}$ commercial red phosphor (integral scope of the emission wavelength: 580 nm–700 nm). The integral emission intensity of $Sr_2Eu_{0.75}La_{0.25}AlO_5$ is found to be 2.5 times higher than that of the $Y_2O_2S:Eu^{3+}$ under 393 nm excitation. The external quantum efficiency of $Sr_2Eu_{0.75}La_{0.25}AlO_5$ and commercial $Y_2O_2S:Eu^{3+}$ red phosphors are measured after excitation at 393 nm and 396 nm, respectively. When the excitation wavelength is 393 nm, the quantum efficiency of $Sr_2Eu_{0.75}La_{0.25}AlO_5$ is 15.6% and $Y_2O_2S:Eu^{3+}$ is 8.7%. When the excitation wavelength is 393 nm, the quantum efficiency of $Sr_2Eu_{0.75}La_{0.25}AlO_5$ is 11.5% and $Y_2O_2S:Eu^{3+}$ is 10.9%. The Chromaticity Coordinates (CIE) of $Sr_2Eu_{0.75}La_{0.25}AlO_5$ is $x=0.64$, $y=0.36$.

4. Conclusions

In conclusion, a series of red phosphors $Sr_2Eu_xLa_{1-x}AlO_5$ ($x=0.05$–1.0) have been synthesized and their luminescent properties are investigated. Upon excitation with UV or near UV light excitation, the phosphor showed strong red emission lines at around 590 nm, 620 nm and 705 nm. The emission intensities initially increase with increasing Eu^{3+} concentration and reach a maximum around $x=0.75$ when excited at 393 nm. The lifetimes are quenched at concentrations around $x=0.75$ also. The quantum efficiency of $Sr_2Eu_{0.75}La_{0.25}AlO_5$ is higher than $Y_2O_2S:Eu^{3+}$ after excitation at 393 nm and 396 nm. The CIE of $Sr_2Eu_{0.75}La_{0.25}AlO_5$ is $x=0.64$, $y=0.36$. The characteristic index shows that the red emission $Sr_2Eu_{0.75}La_{0.25}AlO_5$ phosphor has high color saturation. Preliminary studies showed that this phosphor might have potential applications as a red phosphor for near UV white LEDs.

Acknowledgments

This work is financially supported by the Technology Development Plan of Jilin Province (Grant no.201101106) and the Natural Science Foundation of Changchun Normal University (Grant no. [2009]007 and [2010] 002).

References

[1] M.Y. Wang, J.H. Zhang, X. Zhang, Y.S. Luo, X.G. Ren, S.Z. Lu, X.R. Liu, X.J. Wang, J. Phys. D: Appl. Phys. 41 (2008) 205103.
[2] R.J. Xie, N. Hirosaki, K. Sakuma, Y. Yamamoto, M. Mitomo, Appl. Phys. Lett. 84 (2004) 5404.
[3] S.X. Yan, J.H. Zhang, X. Zhang, S.Z. Lu, X.G. Ren, Z.G. Nie, X.J. Wang, J. Phys. Chem. C 111 (2007) 13256.
[4] H.S. Jang, D.Y. Jeon, Appl. Phys. Lett. 90 (2007) 041906.
[5] N. Hirosaki, R.J. Xie, K. Kimoto, T. Sekiguchi, Y. Yamamoto, T. Suehiro, M. Mitomo, Appl. Phys. Lett. 86 (2005) 211905.
[6] X. Piao, T. Horikawa, H. Hanzawa, K. Machida, Appl. Phys. Lett. 82 (2006) 161908.
[7] Y.H. Song, G. Jia, M. Yang, Y.J. Huang, H.P. You, H.J. Zhang, Appl. Phys. Lett. 94 (2009) 091902.
[8] J.S. Kim, P.E. Jeon, Y.H. Park, J.C. Choi, H.L. Park, G.C. Kim, T.W. Kim, Appl. Phys. Lett. 85 (2004) 3696.
[9] H.S. Jang, D.Y. Jeon, Opt. Lett. 32 (2007) 3444.
[10] J.K. Sheu, S.J. Chang, C.H. Kuo, Y.K. Su, L.W. Wu, Y.C. Lin, W.C. Lai, J.M. Tsai, G.C. Chi, R.K. Wu, IEEE Photonics Technol. Lett. 15 (2003) 18.
[11] X.P. Li, B.J. Chen, R.S. Shen, H.Y. Zhong, L.H. Cheng, J.S. Sun, J.S. Zhang, H. Zhong, Y. Tian, G.T. Du, J. Phys. D: Appl. Phys. 44 (2011) 335403.
[12] Q.Y. Shao, H.J. Li, K.W. Wu, Y. Dong, J.Q. Jiang, J. Lumin. 129 (2009) 879.
[13] M.K. Devaraju, S. Yin, T. Sato, Inorg. Chem. 50 (2011) 4698.
[14] L.H. Yi, X.P. He, L.Y. Zhou, F.Z. Gong, R.F. Wang, J.H. Sun, J. Lumin. 130 (2010) 1113.
[15] M. Drofenik, L. Golic, Acta Crystallogr. B35 (1979) 1059.
[16] R.D. Shannon, Acta Crystallogr. Sect. A 32 (1976) 751.
[17] W.M. Yen, S. Shionoya, H. Yamamoto, Phosphor Handbook 1999204.
[18] S.Y. Zhang, Spectroscopy of Rare Earth Ions 2008111.
[19] J.Y. Sun, H.Y. Du, W.X. Hu, Solid Luminescent Materials 200364.
[20] G.Y. Hong, Luminescent Materials of Rare Earth 201160.
[21] Y.S. Tang, S.F. Hu, C.C. Lin, N.C. Bagkar, R.S. Liu, Appl. Phys. Lett. 90 (2007) 151108.